EQCM study of redox properties of PEDOT/MnO_2 composite films in aqueous electrolytes

Journal of Solid State Electrochemistry (2018) 22_2357ï 2366

A.O. Nizhegorodova[1], S.N. Eliseeva[1], E.G. Tolstopjatova[1], G.G. L§ng[2], D. Zalka[2], M. Ujv§ri[2], V.V. Kondratiev[1*]

[1]Institute of Chemistry, Saint Petersburg State University, 7/9 Universitetskaya nab., Saint Petersburg, 199034, Russia

[2]Institute of Chemistry, Laboratory of Electrochemistry and Electroanalytical Chemistry, Eötvös Loránd University, Pázmány P.s. 1/A, H-1117 Budapest, Hungary

*vkondratiev@mail.ru

- If available, the 16-digit ORCID of the author(s) needed
- M. Ujvari: 0000-0001-9236-9697
- G. Láng: 0000-0002-8362-7671

Abstract

Electrochemical behavior of poly-3,4-ethylenedioxythiophene composites with manganese dioxide (PEDOT/MnO_2) has been investigated by cyclic voltammetry and electrochemical quartz crystal microbalance at various component ratios and in different electrolyte solutions . The electrochemical formation of PEDOT film on the electrode surface and PEDOT/MnO_2 composite film during the electrochemical deposition of manganese dioxide into the polymer matrix was gravimetrically monitored. The mass of manganese oxide deposited into PEDOT at different time of electrodeposition and apparent molar mass values of species, involved into mass transfer during cyclic voltammetry of PEDOT/MnO_2 composites were evaluated. It was found that during the redox cycling of PEDOT/MnO_2 composite films with various MnO_2 content the oppositely directed fluxes of counter ions (anions and cations) occur, resulting in a change of the slope of linear parts of the $\Delta f - E$ plots with changing the mass fraction of MnO_2 in the composite film.

Rectangular shape of cyclic voltammograms of PEDOT/MnO_2 composites with different loadings of manganese dioxide was observed, which is characteristic of the pseudo-capacitive behavior of the composite material. Specific capacity values of PEDOT/MnO_2 composites obtained from cyclic voltammograms were found of about 169 F g^{-1}. The specific capacity, related to the contribution of manganese oxide component, was about 240 F g^{-1}.

Keywords

poly-3,4-ethylenedioxythiophene, manganese oxide, composite materials, cyclic voltammetry, electrochemical quartz crystal microbalance, mass transport

Introduction

Conducting polymers and composites based on the transition metal oxides with conducting polymers are considered as attractive rechargeable electrode materials for electrochemical energy storage [1–8]. In these composite materials, the so-called pseudo-capacitance originates from charge-transfer (Faradaic) processes that take place in the both constituents. A number of conducting polymers, such as polyanilines, polypyrroles and polythiophenes in combination with transition metal oxides, such as RuO_2 [9–11], IrO_2 [12], Co_3O_4 [13–14] and MnO_2 [15–25] were recently proposed as composite electrode materials for electrochemical capacitors. The advantages of manganese dioxide are low cost, environmental compatibility and high specific capacitance. This last property can be better utilized in combination of fine dispersed MnO_2 with conducting polymer matrix. In several papers, the values of capacitance of PEDOT/MnO_2 composites were reported in the range of 148–487 F g^{-1} [17–25].

In particular, PEDOT/MnO_2 composites, obtained by spontaneous redox reaction between reduced PEDOT and MnO_4^- ions [23–25] showed specific capacity values in the range 150–250 F g^{-1} which increased with the increase of MnO_2 loading into the PEDOT film. The calculated specific capacitance values related to contribution of manganese oxide $C_{s,MnO2}$ were in the range 274–310 F g^{-1}, whereas for the PEDOT component they were close to 70–75 F g^{-1}.

24It is known that in a relatively broad potential range (0.0–0.8 V) (e.g. in aqueous $LiClO_4$ solution from about 0.0 V to 0.8 V vs the NaCl saturated calomel electrode (SSCE)), MnO_2 oxide is considered as n-type doping material, whereas PEDOT in this range of potentials acts as p-doping material. (At more positive potentials than 0.8 V vs. SSCE the overoxidation of the polymer may occur [Ujvari M, Gubicza J, Kondratiev V, Szekeres KJ, Láng GG (2015) Morphological changes in electrochemically deposited poly(3,4-ethylenedioxythiophene) films during overoxidation. J Solid State Electrochem 19:1247–1252 , Láng GG, Ujvári M, Vesztergom S, Kondratiev V, Gubicza J, Szekeres KJ (2016) The Electrochemical degradation of poly(3,4-ethylenedioxythiophene) films electrodeposited from aqueous solutions. Z Phys Chem 230:1281–1302].) Due to the different nature of the components of the PEDOT/MnO_2 composite, different counter ions may flux into opposite directions during the oxidation/reduction process. The reduction of MnO_2 in neutral electrolyte solution is supposed to be accompanied by cation flux (surface process of adsorption of cations) [26–30], whereas the reduction of PEDOT is accompanied by anion flux with expulsion of an anion [31]. Therefore it

can be supposed that EQCM measurements could reveal interesting features in mass transport in these composites at redox cycling.

EQCM method is known as one of useful tools for investigation of mass changes during electrochemical synthesis and mass transfer processes, accompanying electrochemical reactions in thin films of electrode modifying layers, in particular, conducting polymers and more complex composite films. The change in the quartz crystal oscillation frequency is very sensitive to mass change during electrochemical synthesis of films and to ion and molecular transport at the film – solution interface. EQCM may give valuable information about stoichiometric mechanism of redox processes taking place in thin films on the quartz crystal electrode.

EQCM has been earlier employed for the study of stoichiometry of mechanism of charge storage in PEDOT and MnO_2 solely, and the contributions of different components of electrolytes into total mass change of PEDOT [31–37] and MnO_2 [26–30] films were established. However, to the best of our knowledge, the charge compensation processes in composite PEDOT/MnO_2 films with different PEDOT:MnO_2 ratios have not been investigated yet during redox cycling in aqueous electrolyte solutions.

In this work, we have investigated the mechanism of charge storage in PEDOT/MnO_2 composites (prepared by electrochemical deposition of manganese oxide into PEDOT) in aqueous $LiClO_4$ and $NaClO_4$ solutions by using a combination of the electrochemical quartz crystal microbalance (EQCM) technique and cyclic voltammetry. Cyclic voltammograms, mass vs. potential and mass vs. charge plots for composite PEDOT/MnO_2 films were systematically investigated and analyzed with the purpose to gain new information about the charge transport processes within these systems.

~~244~~

Experimental

Reagents and Materials

3,4-ethylenedioxythiophene (EDOT, 98%) was purchased from Aldrich. Acetonitrile (HPLC grade, purified cryogenically, water content below 0.008%) was from Cryochrom, Russia. Anhydrous lithium perchlorate ($LiClO_4$) was dried to constant weight. Manganese sulfate ($MnSO_4$) was obtained from Neva Reactive Co., Russia. All other chemicals were of analytical grade. Aqueous solutions were prepared on deionized water of resistivity not less than 18 MΩ, obtained by means of Millipore Direct-Q UV (Millipore Corp., USA) water purification system.

Synthesis of PEDOT and PEDOT/MnO_2

PEDOT films were electrodeposited under galvanostatic conditions (j ~ 1 mA cm^2) [24, 25, 38], from acetonitrile (AN) solution of 0.05 M EDOT and 0.1 M $LiClO_4$. The range of

potential variation during synthesis was 1.1–0.9 V, time of deposition usually was 100 s, if not specified otherwise. All potentials were measured relative to Ag/AgCl reference electrode, Pt foil was used as a counter electrode. The average thickness of the resulting PEDOT films (100s synthesis) calculated based on the amounts of charge consumed during electrodeposition was about 0.3 μm. The Pt-coated quartz crystal (S=1.37 cm^2) was used as the working electrode. The synthesized PEDOT films were thoroughly rinsed by deionized water and then were subjected to the electrodeposition of MnO_2.

Solutions of 0.05M $MnSO_4$ in 0.5M $LiClO_4$ were used for electrochemical deposition of manganese oxide into PEDOT. The deposition process was carried out under constant potential (E = 1.000 V). Each deposition step lasted 100 s, the overall electrodeposition time was varied in the range of 100–600 s.

2.3. Electrochemical measurements

The electrochemical measurements were performed in a three-electrode cell (the cell container was made of glass). The measured potentials are given relative to the NaCl saturated silver chloride electrode (Ag/AgCl). For electrochemical synthesis of PEDOT/MnO_2 composite films on the electrode and for voltammetric measurements, AUTOLAB PGSTAT30 (ECO CHEMIE, The Netherlands) was used. The potential scan rate during cyclic voltammetry (CV) measurements was 5–50 mV s^{-1}. The shape of the cyclic voltammograms (CVs) was stabilized after one to three potential cycles.

EQCM experiments were carried out using the AUTOLAB PGSTAT30 potentiostat interfaced with a QCM200 quartz crystal microbalance system (Stanford Research Systems, USA). PEDOT and PEDOT/MnO_2 was deposited onto the 1.37 cm^2 Pt working electrode of a 1 inch diameter, 5 MHz AT-cut quartz crystal substrate (Stanford Research Systems).

The EQCM measurements were performed with electrochemically synthesized ("pristine") PEDOT films, during the loading of MnO_2 into PEDOT and during redox-processes of PEDOT/MnO_2 composites with different ratios of PEDOT:MnO_2, obtained by consecutive deposition of MnO_2 into the films.

2 Relatively thin PEDOT films were used for the microgravimetric experiments, thus the contribution from the viscoelastic properties of the film to the frequency change was negligible. Further details of the measurements are described in [37].

It is known that the contribution of viscoelastic properties of the polymer film diminishes as the thickness of the polymer film decreases s and EQCM studies are usually performed at a small film thickness to provide such conditions. Therefore, the primary objective was to obtain films of optimum thickness, where the film viscoelastic properties can be neglected and the

mass variation of the electrode with the film is directly proportional to the variation of the crystal resonant frequency. From the technical point of view, the QCM200 instrument allowed monitoring the contribution of viscoelastic properties by changing parameter V_c (the conductance signal related to the series resonance resistance of the quartz crystal by $R_m = 10000 \times 10^{-V_c/5} - 75$ [39]).

Cyclic voltammogram and crystal oscillation frequency were registered simultaneously, together with V_c (using a built-in voltmeter)~~m~~.

According to the calibration experiments performed in media of different viscosity [39], the contribution of viscoelastic interactions between the crystal, film, and electrolyte solution to the crystal oscillation frequency is negligibly low at the R_m values below 925 Ohm. In the course of all experiments (with PEDOT films and PEDOT/MnO_2 composites) , the R_m values did not exceed the above value. This allows assuming that the variation of the crystal oscillation frequency is predominantly related to the film mass variation. The time of film electrodeposition (film thickness) was chosen experimentally with the account for parameter V_c.

Results and discussion

Electrochemical quartz crystal microbalance study of PEDOT films

As already indicated in the introduction, EQCM measurements in this work had two main objectives: 1) study of EQCM responses during the synthesis of the composite film on the electrode, and evaluation of the mass of manganese oxide deposited on the electrode; 2) study of the stoichiometry of the charge-discharge process in the composite film during cycling of potential.

~~2222~~Fig.1 shows the potential transient and the corresponding shift of resonant frequency of electrode during the polymerization of EDOT at constant current density 1 mA cm^{-2}. After a short rise, the potential reached the saturation and slowly decreased near the value 1.17 V, whereas a nearly linear decrease of electrode frequency with time was observed.

The observed small deviations from the linear dependency of frequency (and therefore, mass gain) on time at the initial region of the $f - t$ dependency can be related to the polymer nucleation with formation of a certain critical concentration of oligomers deposited on the electrode surface. In the case of long synthesis times (t > 100 s), deviations of the f–t dependency from linearity also appeared, which can be due to different reasons: different film filling by the solvent, limitations by monomer mass transport towards the surface or a small contribution of the film viscoelastic properties to the frequency response. The observed linearity of the Δf vs. t plot can serve as an indirect confirmation that one can neglect the contribution of the film viscoelastic properties to the frequency response in the chosen range of synthesis times.

The mass gain on the electrode surface was calculated from the frequency change by using Sauerbrey equation:

$$\Delta f = - C_f \cdot \Delta m, \quad (1)$$

where Δf is the frequency variation (Hz), C_f = 56.6 Hz cm^2 g^{-1} is the sensitivity factor of the crystal, Δm is the change in mass per unit area .

The parallel voltammetric and gravimetric responses of a typical pristine PEDOT film in $LiClO_4$ electrolyte are shown in Fig.2. Cyclic voltammograms and mass responses were stable and reproducible during prolonged cycling.

The frequency – potential dependencies obtained at different scan rates are shown in Fig.3. The monotonic almost linear change of electrode frequency with potential was observed with small hysteresis for forward and back scan of potential. The oxidation of PEDOT film in the forward scan is followed by a decrease of frequency, which indicates an increase of the film mass, the reduction of PEDOT in the reverse scan, is followed by an increase of frequency, therefore, a decrease in mass occurs. Lower hysteresis between the forward and back scans was observed with decrease of scan rate.

The observed dependency of the frequency shift from the electrode potential is qualitatively consistent with the mechanism of doping/dedoping of PEDOT films, where oxidation of the film is accompanied by an increase in the mass of the electrode due to the uptake of the dopant anions (perchlorate ions) into the film, and the reverse reduction process – the release of the anions from the film.

The linear mass – charge dependency with constant slope indicates the constancy of apparent molecular mass (M_{app}) of the transferred species.

$$M_{app} = z\, F\, \Delta m/\Delta Q \quad (2)$$

where M_{app} – apparent mass of species (cations, anions and solvent molecules), taking part in the overall mass transport process.

The calculated value of apparent molar mass M_{app} = 80.3 g mol^{-1} is significantly (by about 10%) lower than the theoretical mass of ClO_4^- ions, which are expected as counter-ions. Nevertheless, this value is in good agreement with those (80 g mol^{-1} and 82 g mol^{-1}) reported previously in [35,37].

Cyclic voltammetric and EQCM study of PEDOT/MnO_2 composites

EQCM measurements during the deposition of MnO_2 into PEDOT films

As described in the "Experimental" section the electrochemical deposition of manganese dioxide was performed by the well known method of electrooxidation of manganese (II) ions according to the overall reaction:

$$Mn^{2+} + 2H_2O \rightarrow MnO_2 + 4H^+ + 2e^- \quad (3)$$

The formation of PEDOT/MnO_2 composite film during the electrochemical deposition of manganese dioxide into the polymer matrix was gravimetrically monitored.

Fig.4 shows the current response and resonant frequency shifts of the electrode during the potentiostatic deposition of MnO_2 into PEDOT film from the aqueous solution of 0.05 M $MnSO_4$ and 0.5 M $LiClO_4$. The consecutive deposition of manganese oxide into the film was carried out under the conditions described above, each deposition step lasted for 100 seconds.

The amounts of MnO_2 deposited into the PEDOT film were calculated from the shift of the crystal oscillation frequency in accordance with the Sauerbrey equation. Fig. 5a shows the mass gain versus deposition time dependencies during the individual deposition steps. As it can be seen from the figure , when the manganese oxide is deposited into the film, the change (increase) of the mass of the electrode over time is essentially linear, therefore it seems reasonable to suppose that the deposition rate (i.e. the slope $d\Delta m/dt$) is practically constant over the range of superficial masses studied. ~~2~~

In addition, for the first several steps, a fairly linear relationship between the mass of MnO_2 deposited into the film and the "total" deposition time became apparent (Fig. 5b). The difference in mass of the composite and initial PEDOT films allow to estimate the mass of the deposited MnO_2. The calculated masses are shown in Table 1.

Cyclic voltammetry of the PEDOT/MnO_2 composite films

Cyclic voltammograms of PEDOT/MnO_2 composites with different loadings of manganese dioxide (recorded in 1 M $LiClO_4$ solution (???) at the scan rate of 10 mV/s) are shown in Fig. 6. Nearly ideal rectangular shaped cyclic voltammograms without any current peaks were observed for both the initial PEDOT and PEDOT/MnO_2 composite electrodes in the whole potential range . The shape of the cyclic voltammograms (characteristic for pseudocapacitive behavior) suggests that the rate of the charge-discharge processes is high. On the other hand, the (near linear) increase of of the charging current with the MnO_2 content in composite film is a result of the pseudocapacitive contribution of both components. The CV shape became slightly distorted at the edges of the voltammograms and these distortions are more obvious with increase of manganese oxide loading. This effect, indicating a significant increase in the resistance of the manganese oxide layer and a decrease in its redox efficiency, was especially pronounced at higher potential scan rates.

On the other hand, the effect of the potential scan rate on cyclic voltammograms of PEDOT/MnO_2 composite films is also quite interesting. The (pseudo-)capacitive charging/discharging currents increase with increasing the scan rate. Moreover, a directl proportionality between the current and the scan rate was observed at any potentials around the middle of the potential range in which the cycling was done. The cathodic and anodic charges were practically identical and their ratio was independent of the scan rate, which indicates the reversibility of the charge / discharge processes. It is evident from the scan rate normalized CVs shown in Fig.8 , that in spite of a relatively high content of manganese dioxide in the composite (PEDOT/MnO_2(600) with 57 wt.% of MnO_2), the rate of charging/discharging processes in the PEDOT/MnO_2 composite (including the processes associated with the oxidation/reduction of the polymer, and the redox processes in the dispersed manganese oxide particles). Moreover, the dependence of the current on the scan rate in this region is linear for both the PEDOT/MnO_2 /1M $LiClO_4$(aq.) and the PEDOT/MnO_2 /1M $NaClO_4$(aq.) electrodes, which is consistent with the (pseudo-)capacitive charging behavior. 4. The specific capacity values of composite films were evaluated from the CV-s recorded at the scan rate of 50 mV s^{-1}. . The calculated specific capacity of the composite material was about 169 F g^{-1} for the PEDOT/MnO_2 (600 s) electrode, whereas the specific capacity, related to the contribution of MnO_2 was about 240 F g^{-1}. These values are comparable with those reported in the literature for similar PEDOT/MnO_2 composites [17-23].

EQCM study of PEDOT/MnO_2 composite films

Fig. 7 illustrates the effect of the electrode potential on the resonant frequency of the quartz crystal covered with PEDOT/MnO_2 composite films prepared by consecutive electrochemical deposition of manganese dioxide. It can be clearly seen that the slopes of the linear regions of the frequency change (Δf) vs. electrode potential (E) curves change considerably with increasing MnO_2 mass fraction in the composite film. For an easier comparison of the results, all Δf *vs.* E curves corresponding to the PEDOT/MnO_2 samples with different MnO_2 content start at the same point ($\Delta f = 0$ on the vertical axis in Fig. 7). 2 2 22 The reproducibility of the EQCM measurements was good, consecutive potential cycles provided highly reproducible $\Delta f\,(E)$ dependencies for each sample. Visualization of the data (Fig. 7) reveals that the $\Delta f - E$ relationships are close to linear in a fairly broad potential range with varying degree of hysteresis between forward and reverse scans. 2

Nevertheless, this type of behavior is quite unusual for “simple” modified electrodes and can presumably be attributed to charge and mass transport in the film associated with redox processes in/at the Mn-containing particles. 22In a general case, we have to consider all

oxidation-reduction (redox) processes occurring in the composite film. On the other hand we have to take into account that both the PEDOT and the Mn-containing phase may contribute to the mass change in distinct ways. [2] As a result, the interpretation of the EQCM information presents a number of difficulties.

A possible explanation of the observed results is as follows. As it was reported in previous papers [31, 32, 35, 36], the charge compensating process during the oxidation of PEDOT film mainly comprises the insertion of anions into the film. On the other hand, the oxidation process of the manganese oxide [+] component (represented by the chemical formula $MnOO^-C^+$, where the symbol C^+ stands for a single charged cation originating from the electrolyte solution which may be adsorbed on, or absorbed/intercalated in manganese oxide particles) in the region 0–0.8V vs. Ag/AgCl/(saturated aqueous NaCl-solution) includes the surface oxidation of manganese ions Mn(III) to Mn(IV) followed by the desorption of C^+-ions which leave the film structure and enter the solution [26–29].

The corresponding simplified electrode reactions taking place at redox cycling can be written as:

$$Mn^{(IV)}O_2 + xe + xC^+ = C_x^+ \, Mn^{(III)}_x Mn^{(IV)}_{1-x} O_2 \qquad (4)$$

$$(PEDOT^+ \cdot A^-) + e = PEDOT^0 + A^- \qquad (5)$$

In both reactions a number of solvent molecules can be involved in the mass transfer processes, therefore the total mass change (Δm_{tot}) can written as follows:

$$\Delta m_{tot} = \Delta m_{A^-} + \Delta m_{C^+} + \Delta m_s \qquad (6)$$

where Δm_{A^-} is the change in mass (with respect to a suitably chosen reference state) due to the flux of anions, Δm_{C^+} is the change in mass due to the flux of cations, and Δm_s is the mass change due to the solvent transport, respectively.

In this case, comprising fluxes of cations, anions and solvent molecules, the analysis of individual contributions (of different particles) to overall flux faces difficulties.

As it was shown earlier in refs. [26,27] (where the apparent masses of charge compensating ions or “counterions” were evaluated by using the EQCM technique), the redox process in MnO_2 films involves the transport of one water molecule into the manganese oxide lattice [26, 27]. For PEDOT films in aqueous solutions, the obtained M_{app} values, to a first approximation, are close to the molar mass of the charge compensating ions and the molar mass of 1-2 transferred water molecules (depending on the composition of the electrolyte solution) [31, 32, 35, 36].

~~app2~~Therefore, the M_{app} values that can be obtained for the PEDOT/MnO_2 composites with different loadings of manganese dioxide are also influenced by the number of solvent molecules transferred by counter-moving counter-charged ions. Nevertheless, Eq.(6) can be written as

$$\Delta m_{tot} = \Delta m_{A^-} + \Delta m_{C^+} + \Delta m_s = (\Delta m_{A^-} + \Delta m_{s,A^-}) + (\Delta m_{C^+} + \Delta m_{s,C^+}), \qquad (6a)$$

where $\Delta m_{s,A^-}$ is the mass change caused by the solvent molecules associated with the movement of anions and $\Delta m_{s,C^+}$ is the mass change caused by the solvent molecules associated with the movement of cations. Eq.(6a) can be written more simply as

$$\Delta m_{tot} = \Delta m_{-} + \Delta m_{+} \ , \qquad (7)$$

with $\Delta m_{-} = \Delta m_{C^+} + \Delta m_{s,C^+}$ and $\Delta m_{+} = \Delta m_{A^-} + \Delta m_{s,A^-}$. (As an even rougher approximation we may equate Δm_{-} and Δm_{+} with Δm_{A^-} and Δm_{C^+}, respectively.)

Equation (7) can provide a basis for a simplified semi-quantitative description of the observed phenomena. The total (molar) mass flux of transported species (J_{tot}) normalized to the piezoelectrically active surface area of the quartz crystal can be given as:

$$j_{tot} = \frac{d\Delta m_{tot}}{dtM} \ \text{~~C+A-~~}$$

$$J_{tot} = \frac{d\Delta m_{tot}}{M_x dt} = \frac{d\Delta m_{+}}{M_{+} dt} + \frac{d\Delta m_{-}}{M_{-} dt}, \qquad (8)$$

where M_x is an apparent molar mass of the species involved in the charge compensation process during oxidation or reduction of the film, M_{-} and M_{+} are the apparent molar masses of the anion and the cation, $\frac{d\Delta m_{+}}{M_{+} dt} = \frac{d\Delta n_{C^+}}{dt}$ and $\frac{d\Delta m_{-}}{M_{-} dt} = \frac{d\Delta n_{A^-}}{dt}$ are the molar fluxes of cations and anions, respectively. (It should be stressed here that x is a hypothetical entity, which is best defined as an ionic species with a charge number of z_x.)

The flux is positive for species that enter the film (i.e. which are inserted into composite material) and is negative for species that leave the film. The apparent molar mass of charge compensating ions can be evaluated from the slope of the mass change (Δm_i) vs. charge (Q) curve in accordance with the equation

$$M_{i,app} = z_i F \frac{d\Delta m_i}{dQ}. \qquad (9)$$

(In Eq.(9) z_i denotes the charge number of species i.) Combination of Eqs. (8) and (9) gives

$$\frac{d\Delta m_{tot}}{M_x dt} = \frac{M_x dQ}{z_x F dt} = \frac{M_x i}{z_x F} \qquad (10)$$

where ~~x~~ i is the current density.

The total charge passed through the electrode can be expressed as a sum of charges originating from the individual processes

$$dQ = |dQ_-| + |dQ_+| . \quad (11)$$

Since the oppositely-charged ions move in opposite directions, from Eq.(7) one obtains:

$$d\Delta m_{tot} = |d\Delta m_-| - |d\Delta m_+| , \quad (12)$$

By combining Eqs.(9)–(12) we get

$$\frac{M_x dQ}{z_x F} = \frac{M_- dQ_-}{z_- F} - \frac{M_+ dQ_+}{z_+ F} , \quad (13)$$

and with finite changes in the charge variables:

$$\frac{M_x}{z_x F} = \frac{\Delta Q_-}{z_- F \Delta Q} M_- - \frac{\Delta Q_+}{z_+ F \Delta Q} M_+ . \quad (14)$$

Since in the present case $z_+ = z_-$, by taking into account Eq.(11), Eq.(14) can be rewritten as

$$M_x = \alpha M_- - (1-\alpha) M_+ , \quad (15)$$

where $\alpha = \Delta Q_- / \Delta Q$ is the fraction of total charge compensated by anions, and $1-\alpha = \Delta Q_+ / \Delta Q$ is the fraction of total charge compensated by cations.

Eq.(15) provides a relationship between the experimentally obtained apparent molar mass of the charge carrier x (i.e. the ionic species entering or leaving the film) and the (apparent) molar masses of individual ions – anions M_- and cations M_+.

The data presented in Fig. 7 (potential sweep rate v=10 mV s^{-1}) and a similar set of data for v=20 mV s^{-1} were analyzed in terms of $\Delta m - \Delta Q$ dependencies. The apparent molar mass M_x was calculated using the slopes from the linear parts of the Δm vs. ΔQ plots in accordance with Eq.(9).

The calculated values of the apparent molar mass of the charge carriers are shown in Table 2.

The presented data shows that the counter-ion mass is almost independent of the potential scan rate (10 and 20 mV/s) for composite films of all compositions. With the increase of MnO_2 mass in the composite film the gradual decrease of the apparent molar mass (M_x) values from about 80 g mol^{-1} (the value calculated for the pure PEDOT film, which is close to the molar mass of perchlorate anions) to about −8 g mol^{-1} was observed for the oxidation process in 1 M $LiClO_4$ solution. The observed changes in the apparent molar masses are qualitatively consistent with the prevailing uptake of dopant anions (perchlorate ions) into the film during the oxidation of pristine PEDOT films, whereas at high MnO_2 content the

prevailing mass transfer process during the oxidation of the composite films is the expulsion of cations from the manganese oxide component.

At low loadings of manganese dioxide , the negative slope of the Δf vs. E curves in Fig. 7 (increase of mass during oxidation) indicates the predominant role of perchlorate ions in the redox mechanism of the PEDOT/MnO_2 composite film (doping-dedoping process), i.e. the flux of this ion is the net residual ion flux. With an increase in the mass fraction of manganese dioxide, the situation is gradually changing and the contribution of the cations to the total ion flux begins to increase. Up to about 50 m/m% MnO_2 loading anion and cation fluxes tend to equalize. For PEDOT/MnO_2(400) composite with 47 wt.% of MnO_2 (see Table 1), the fluxes of cations and anions ("doping/dedoping particles") are almost equal and the mass of the composite film hardly changes during the oxidation/reduction process. With a further increase in the mass fraction of MnO_2 in the composite, the sign of the slope of the Δf vs. E curve changes from negative to positive , and the predominant contribution to the change of the mass of the composite during the oxidation/reduction process is made by manganese dioxide recharging and the associated desorption/sorption of electrolyte cations.

~~22224~~The results of simultaneous cyclic voltammetry and EQCM measurements carried out in 1 M $NaClO_4$ solution are also consistent with the above considerations. The cyclic voltammograms of PEDOT/MnO_2 composite films recorded at the same scan rates in 1 M $NaClO_4$ and 1 M $LiClO_4$ are practically identical (Fig. 9a). As it was discussed earlier, the cation of electrolyte takes part in the charge/discharge process of manganese dioxide. Therefore, the comparable current values in the two selected alkali perchlorate solutions with a big difference in the mass and size of the alkali metal cations (M_{Li^+}= 7 g mol^{-1}, M_{Na^+}= 23 g mol^{-1}) indicates the high dispersity of manganese dioxide in the composite and the predominancy of the surface charge exchange reaction. One may speculate that the slightly higher current in the $LiClO_4$ solution is due to intercalation of Li^+ ions into the MnO2 structure, however, one has to be careful not to overinterpret the results, especially because there are several alternative explanations for these small differences.

Fig. 9b shows that during potential cycling of the same composite PEDOT/MnO_2(600) film in the two different electrolyte solutions (1M $LiClO_4$ and 1M $NaClO_4$), the shapes of the resonant frequency vs. potential curves are similar, but the slopes of the curve measured in 1M $NaClO_4$ solution are always higher at identical potential values than those of the other curve. The shape change is similar to that observed in the case of increasing the mass fraction of manganese dioxide in the composite film. These results confirm once again the prevailing participation of the cation in the charging/discharging process of the MnO_2 - rich composite film.

Changing the molar mass of transferred counter-ions on changing the electrolyte is also reflected in Table 2. In the case of the PEDOT/MnO_2(600) composite film the apparent molar mass of transferred counter-ions changes from −8.3 g mol^{-1} (determined at a scan rate v = 10 mV·s^{-1}) or -6.7 g mol^{-1} (determined at v = 20 mV·s^{-1}) in 1 M $LiClO_4$ to −16.7 g mol^{-1} (determined at v = 10 mV·s^{-1}) or -15.8 g mol^{-1} (determined at v = 20 mV·s^{-1}) in 1M $NaClO_4$, respectively. This can be explained by the increase in mass of the cation (from 7 g mol^{-1} for Li^+ to 23 g mol^{-1} for Na^+) released from the film upon oxidation 2.

The complex nature of the process under study, simultaneous transfer of doping/dedoping anions and cations, as well as the solvent molecules involved into the redox processes, incomplete redox transformations of manganese oxide incorporated into the film, etc., makes a more quantitative analysis of EQCM data extremely complicated. Nevertheless, taken together, the obtained data suggest that during the charge-discharge process in the composite film bidirectional fluxes of mass occur, and manganese oxide oxidation/reduction proceeds with the transfer of supporting electrolyte cations into the film.

Conclusion

Monitoring of mass change by EQCM during the electrochemical synthesis and redox transformation of PEDOT/MnO_2 composite films was performed. It was found that reversible mass change during redox cycling takes place and the shapes of frequency–potential curves depend on the composition of the PEDOT/MnO_2 film. The analysis of Δf–E dependencies revealed that the redox process in the composites is accompanied by mixed cation and anion transport, oppositely directed fluxes of counter ions (anions and cations) occur, and the individual ion fluxes depend on the composition of the composite material The coexistence of these two fundamental, but oppositely directed mass movements constitutes one of the most essential phenomena in the films, and results in the change of the slope of linear parts of Δf vs. E curves with increasing the mass fraction of manganese oxide 2. At small fractions of MnO_2 in the PEDOT/MnO_2 composite film the flux of anions is predominant, while in the opposite case (i.e. at high fractions of MnO_2), the predominant flux of cations is observed 2. Rectangular shaped cyclic voltammograms, characteristic of the pseudo-capacitive behavior, were observed for 2 composites with different loadings of manganese dioxide. Specific capacity values of PEDOT/MnO_2 composites were found of about 169 F g^{-1}, and the specific capacity related to the contribution of manganese oxide component, was about 240 F g^{-1}.

Acknowledgements

Support of the Russian Foundation for Basic Research, grant № 16-03-00457, and the Hungarian

National Research, Development and Innovation Office – NKFI-OTKA (grants Nos. K 109036 and VEKOP-2.3.2-16-2017-00013, co-financed by the European Regional Development Fund) is gratefully acknowledged.

References

1. Snook GA, Kao P, Best AS (2011) Conducting-polymer-based supercapacitor devices and electrodes. J Power Sources 196:1–12

2. Yu G, Xie X, Pan L, Bao Z, Cui Y (2013) Hybrid nanostructured materials for high performance electrochemical capacitors. Nano Energy 2:213–234

3. Holze R, Wu YP (2014) Intrinsically conducting polymers in electrochemical energy technology: Trends and progress. Electrochim Acta 122:93–107

4. Holze R (2017) Metal Oxide/Conducting Polymer Hybrids for Application in Supercapacitors. In: Dubal DP, Romero PG, Korotcenkov G (eds) Metal Oxides in Supercapacitors, Elsevier, Amsterdam, pp 219–245

5. Lokhande VC, Lokhande AC, Lokhande CD, Kim JH, Ji T (2016) Supercapacitive composite metal oxide electrodes formed with carbon, metal oxides and conducting polymers. J Alloys Compd 682:381–403

6. Naoi K, Morita M (2008) Advanced polymers as active materials and electrolytes for electrochemical capacitors and hybrid capacitor systems. Electrochem Soc Interfaces 17:44–48

7. Snook GA, Peng C, Fray DJ, Chen GZ (2007) Achieving high electrode specific capacitance with materials of low mass specific capacitance: Potentiostatically grown thick micro-nanoporous PEDOT films. Electrochemistry Communications 9:83–88

8. Meng Q, Cai K, Chen Y, Chen L (2017) Research progress on conducting polymer based supercapacitor electrode materials. Nanoenegry 36:268–285

9. Hu CC, Chang KH, Lin MC, Wu YT (2006) Design and tailoring of the nanotubular arrayed architecture of hydrous RuO_2 for next generation supercapacitors. Nano Letters 6:2690-2695

10. Subramanian V, Hall SC, Smith PH, Rambabu B (2004) Mesoporous anhydrous RuO_2 as a supercapacitor electrode material. Solid State Ionics 175:511–515

11. Zheng JP, Cygan PJ, Jow TR (1995) Hydrous ruthenium oxide as an electrode material for electrochemical capacitors. J Electrochem Soc 142:2699–2703

12. Liu DQ, Yu SH, Son SW, Joo SK (2008) Electrochemical performance of iridium oxide thin film for supercapacitor prepared by radio frequency magnetron sputtering method. ECS Transactions 16:103–109

13. Pawar SA, Patil DS, Shin JC (2017) Hexagonal sheets of Co_3O_4 and Co_3O_4-Ag for high-performance electrochemical supercapacitors. J Ind Eng Chem 54:162–173

14. Du W, Liu R, Jiang Y, Lu Q, Fan Y, Gao F (2013) Facile synthesis of hollow Co_3O_4 boxes for high capacity supercapacitor. J Power Sources 227:101–105

15. Bélanger D, Brousse T, Long JW (2008) Manganese oxides: Battery materials make the leap to electrochemical capacitors. Electrochem Soc Interfaces 17:49–52

16. Yang Y, Yuan W, Li S, Yang X, Xu J, Jiang Y (2015) Manganese dioxide nanoparticle enrichment in porous conducting polymer as high performance supercapacitor electrode materials. Electrochim Acta 165:323–329

17. Tang PY, Zhao YQ, Xu CL (2013) Step-by-step assembled poly(3,4-ethylenedioxythiophene)/manganese dioxide composite electrodes: Tuning the structure for high electrochemical performance. Electrochim Acta 89:300–309

18. Rios EC, Correa AA, Cristovan FH, Pocrifka LA, Rosario AV (2011) Poly(3,4-ethylenedioxithiophene)/MnO_2 composite electrodes for electrochemical capacitors. Solid State Sci 13:1978–1983

19. Liu R, Lee R, Lee SB (2008) MnO_2/Poly(3,4-ethylenedioxythiophene) coaxial nanowires by one-step coelectrodeposition for electrochemical energy storage. J Am Chem Soc 130:2942–2943

20. Babakhani B, Ivey DG (2010) Improved capacitive behavior of electrochemically synthesized Mn oxide/PEDOT electrodes utilized as electrochemical capacitors. Electrochim Acta 55:4014–4024

21. Liu R, Duay J, Lee SB (2011) Electrochemical formation mechanism for the controlled synthesis of heterogeneous MnO_2/Poly(3,4-ethylenedioxythiophene) nanowires // ACS Nano 5:5608–5619

22. Sen PT, De A, Chowdhury AD, Bandyopadhyay SK, Agnihotri N, Mukherjee M (2013) Conducting polymer based manganese dioxide nanocomposite as supercapacitor. Electrochim Acta 108:265–273

23. Liu R, Duay J, Lee SB (2010) Redox exchange induced MnO_2 nanoparticle enrichment in poly(3,4-ethylenedioxythiophene) nanowires for electrochemical energy storage. ACS Nano 4:4299–4307

24. Nizhegorodova AO, Kondratiev VV (2014) Synthesis and electrochemical properties of composite materials based on poly-3,4-ethylenedioxythiophene with manganese dioxide inclusions. Russ J Electrochem 50:1157–1163

25. Tolstopjatova EG, Eliseeva SN, Nizhegorodova AO, Kondratiev VV (2015) Electrochemical properties of composite electrodes, prepared by spontaneous deposition of manganese oxide into poly-3,4-ethylendioxythiophene. Electrochim Acta 173:40–49

26. Arias CR, Debiemme-Chouvy C, Gabrielli C, Laberty-Robert C, Pailleret A, Perrot H, Sel O (2014) New insights into pseudocapacitive charge-storage mechanisms in Li-birnessite type MnO_2 monitored by fast quartz crystal microbalance methods. J Phys Chem C 118:26551–26559

27. Kuo SL, Wu NL (2006) Investigation of pseudocapacitive charge storage reaction of MnO_2•nH_2O supercapacitors in aqueous electrolytes. J Electrochem Soc 153:A1317−A1324

28. Chu YH, Hu CC, Chang KH (2012) Electrochemical quartz crystal microbalance study of amorphous MnO_2 prepared by anodic deposition. J Electroanal Chem 685:37–40

29. Devaraj S, Munichandraiah N (2009) EQCM investigation of the electrodeposition of MnO_2 and its capacitance behavior. Electrochem Solid-State Lett 12:F21–F25

30. Ye Q, Dong R, Xia Z, Chen G, Wang H, Tan G, Jiang L, Wang F (2014) Enhancement effect of Na ions on capacitive behavior of amorphous MnO_2. Electrochim Acta 141:286–293

31. Bund A, Neudeck S (2004) Effect of the solvent and the anion on the doping/dedoping behavior of poly(3,4-ethylenedioxythiophene) films studied with the electrochemical quartz microbalance. J Phys Chem B 108:17845–17850

32. Hillman AR, Daisley SJ, Bruckenstein S (2007) Kinetics and mechanism of the electrochemical p-doping of PEDOT. Electrochem Commun 9:1316–1322

33. Hillman AR, Daisley SJ, Bruckenstein S (2007) Solvent effects on the electrochemical p-doping of PEDOT. Phys Chem Chem Phys 9:2379–2388

34. Niu L, Kvarnstrom C, Ivaska A (2004) Mixed ion transfer in redox processes of poly(3,4-ethylenedioxythlophene). J Electroanal Chem 569:151–160

35. Efimov I, Winkels S, Schultze JW (2001) EQCM study of electropolymerization and redox cycling of 3,4-polyethylenedioxythiophene. J Electroanal Chem 499:169–175

36. Plieth W, Bund A, Rammelt U, Neudeck S, Duc LM (2006) The role of ion and solvent transport during the redox process of conducting polymers. Electrochim Acta 51:2366–2372

37. Eliseeva SN, Babkova TA, Kondratiev VV (2009) Mass transfer of ions and solvent at redox processes in poly-3,4-ethylenedioxythiophene films. Russ J Electrochem 45:152–159

38. Tolstopyatova EG, Pogulaichenko NA, Eliseeva SN, Kondratiev VV (2009) Spectroelectrochemical study of poly-3,4-ethylenedioxythiophene films in the presence of different supporting electrolytes. Russ J Electrochem 45:252–262

39. QCM200. Operation and Service Manual. Stanford Research Systems, Inc., 2004.

40. Ujvari M, Gubicza J, Kondratiev V, Szekeres KJ, Láng GG (2015) Morphological changes in electrochemically deposited poly(3,4-ethylenedioxythiophene) films during overoxidation. J Solid State Electrochem 19:1247–1252.

41. Láng GG, Ujvári M, Vesztergom S, Kondratiev V, Gubicza J, Szekeres KJ (2016) The Electrochemical degradation of poly(3,4-ethylenedioxythiophene) films electrodeposited from aqueous solutions. Z Phys Chem 230:1281–1302

Figure captions

Fig.1 Galvanostatic synthesis of PEDOT film on Pt-coated quartz crystal: *E–t* dependency and frequency change during PEDOT synthesis from solution of 0.05 M EDOT, 0.1 M $LiClO_4$ in acetonitrile (AN)

Fig. 2 CV (solid line) and Δf–*E* dependency (dotted line) of a pristine PEDOT film in 1 M $LiClO_4$ (v=20 mV s^{-1})

Fig. 3 The frequency – potential dependencies for PEDOT films at different scan rates (v=5–50 mV s^{-1})

Fig. 4 Current (solid line) and frequency (dashed line) changes with time during potentiostatic deposition of MnO_2 into PEDOT film electrode

Fig. 5 Deposition of MnO_2 from aqueous solution of 0.05M $MnSO_4$ and 0.05M $LiClO_4$. ***a*** – Deposition time dependence of mass gain of MnO_2 during the electrochemical deposition into PEDOT film, 1–6: number of 100-second deposition steps; ***b*** – The relationship between the mass of MnO_2 incorporated into PEDOT film and the time of deposition. 44

Fig. 6 Cyclic voltammograms (v = 10mV s^{-1}) for PEDOT and PEDOT/MnO_2 composite films with different times of consecutive MnO_2 deposition. MnO_2 deposition time for each new deposition step was 100s.

Fig. 7 Δf–*E* dependencies for PEDOT and PEDOT/MnO_2 composite films with different times of consecutive MnO_2 deposition. MnO_2 deposition time for each new deposition step was 100s, v = 10 mV s^{-1}

Fig. 8 Normalized cyclic voltammograms of PEDOT/MnO_2(600) electrode. *v,* mV s^{-1}: ***1****–10;* ***2****–20;* ***3****–50.* Solution: 1M $LiClO_4$

Fig. 9 ***a*** **–** cyclic voltammograms (v=50 mV s^{-1}) and ***b*** **–** Δf–*E* dependencies of PEDOT/MnO_2(600) electrode in: ***1***. 1M $LiClO_4$; ***2.*** 1M $NaClO_4$ solutions, respectively

Table 1 EQCM data for PEDOT/MnO_2 composites with different times of MnO_2 deposition

Table 2 Apparent molar mass of charge carriers during PEDOT/MnO_2 oxidation at different potential scan rates

Composite (MnO_2 deposition time, s)	Composite mass, μg	MnO_2 mass, μg	MnO_2, wt.%	MnO_2 mass gain after 100 s of consecutive deposition, μg
PEDOT	159	–	–	–
PEDOT/MnO_2 (100)	193	33	17	33
PEDOT/MnO_2 (200)	228	68	31	35
PEDOT/MnO_2 (300)	265	105	39	37
PEDOT/MnO_2 (400)	303	143	47	38
PEDOT/MnO_2 (500)	340	180	53	37
PEDOT/MnO_2 (600)	371	211	57	31

Table 1 EQCM data for PEDOT/MnO_2 composites with different times of MnO_2 deposition

Material, electrolyte	Apparent molar mass of charge carriers, M_{app}	
	20 mV s^{-1}	10 mV s^{-1}
PEDOT, 1M $LiClO_4$	78.9	80.3
PEDOT/MnO_2(100), 1M $LiClO_4$	35.5	35.4
PEDOT/MnO_2(200), 1M $LiClO_4$	16.2	15.4
PEDOT/MnO_2(300), 1M $LiClO_4$	6.4	5.4
PEDOT/MnO_2(400), 1M $LiClO_4$	1.0	0.9
PEDOT/MnO_2(500), 1M $LiClO_4$	-3.0	-4.8
PEDOT/MnO_2(600), 1M $LiClO_4$	**-6.7**	**-8.3**
PEDOT/MnO_2(600), 1M $NaClO_4$	**-15.8**	**-16.7**

Table 2. Apparent molar mass of charge carriers during PEDOT/MnO_2 oxidation at different potential scan rates

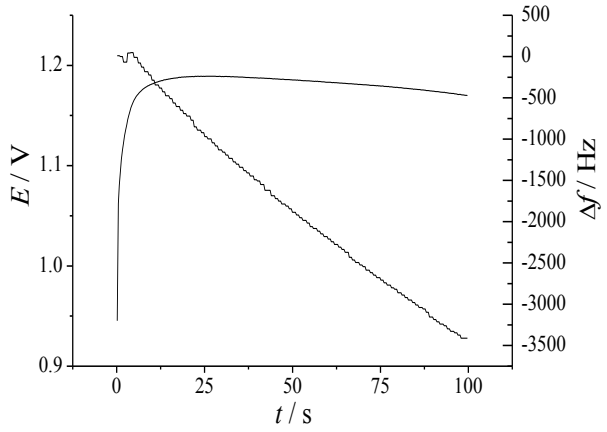

Fig.1 Galvanostatic synthesis of PEDOT film on Pt-coated quartz crystal: *E, t*-dependency and frequency change during PEDOT synthesis from solution of 0.05 M EDOT, 0.1 M $LiClO_4$ in AN.

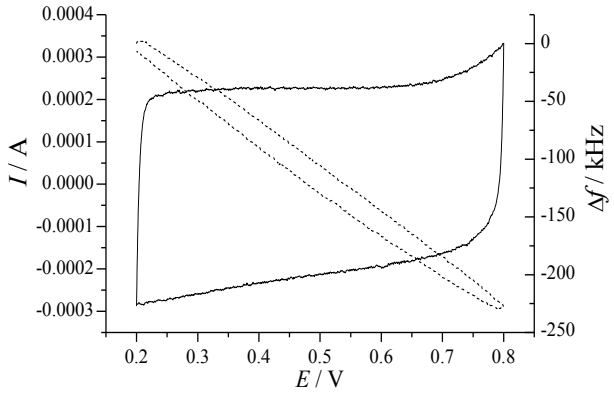

Fig. 2 CV and Δ*f*–*E* dependencies of a pristine PEDOT film in 1 M $LiClO_4$ (v=20 mV s^{-1})

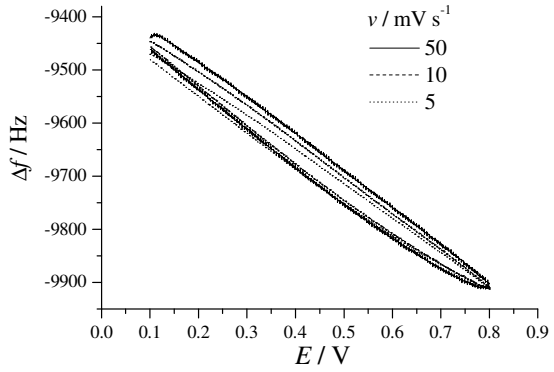

Fig. 3 The frequency – potential dependencies for PEDOT films at different scan rates (v=5–50 mV s^{-1})

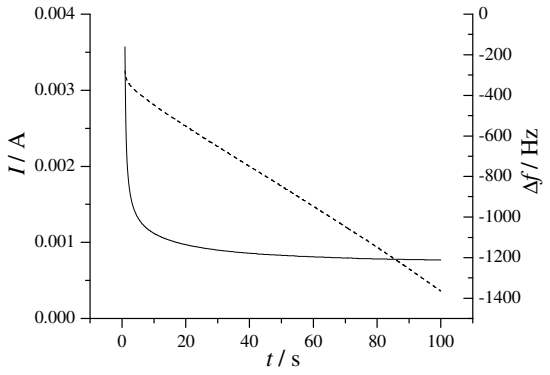

Fig.4 Current (solid line) and frequency (dashed line) changes with time during potentiostatic deposition of MnO_2 into PEDOT film electrode

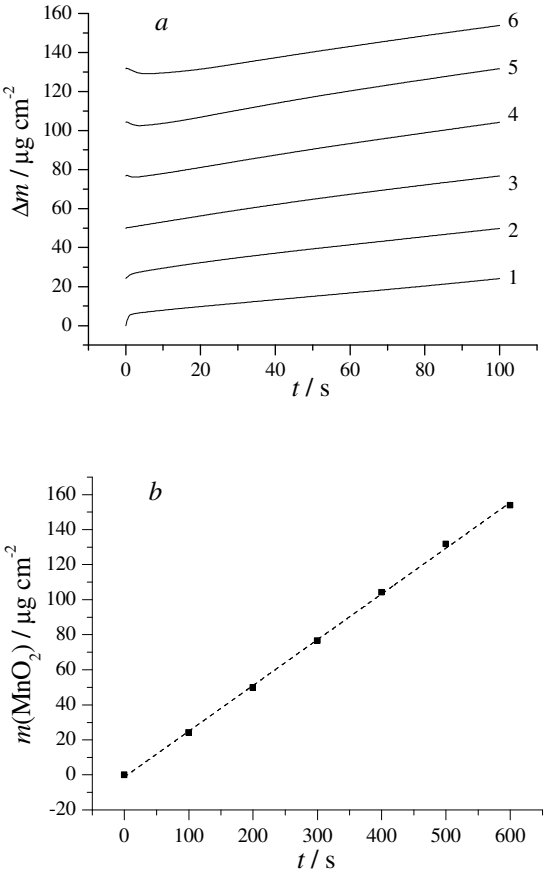

Fig. 5 a – Dependence of mass gain of MnO_2 during the electrochemical deposition into PEDOT film from the time of deposition, 1-6: number of a 100-second deposition step; **b** – The relationship between the mass of MnO_2, incorporated into PEDOT film and the time of deposition. Deposition from an aqueous solution of 0.05M $MnSO_4$, 0.05M $LiClO_4$.

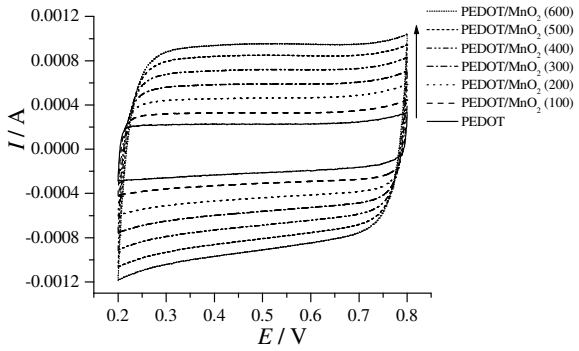

Fig. 6 Cyclic voltammograms (ν = 10mV s^{-1}) for PEDOT and PEDOT/MnO_2 composite films with different times of consecutive MnO_2 deposition. MnO_2 deposition time for each new deposition step was 100s

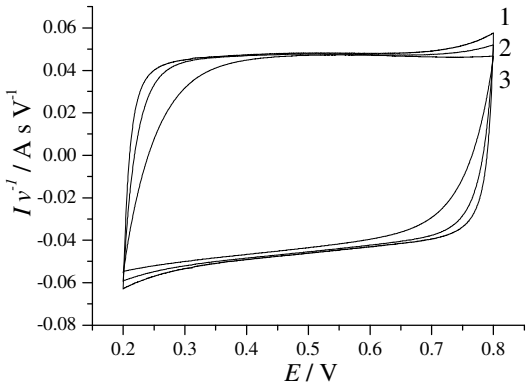

Fig. 8 Normalized cyclic voltammograms of PEDOT/MnO_2(600) electrode. *v,* mV s^{-1}: ***1****–10;* ***2****–20;* ***3****–50.* 1M $LiClO_4$

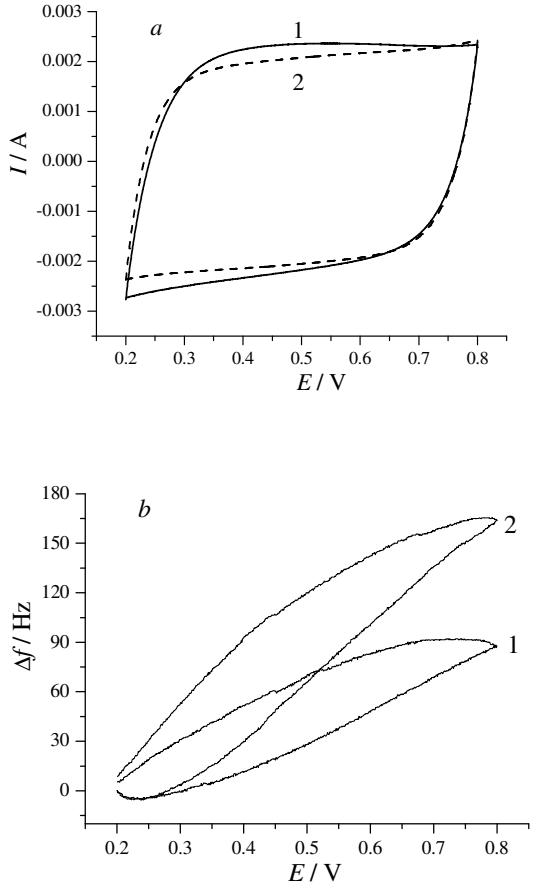

Fig. 9 ***a-*** cyclic voltammograms (v=50 mV s^{-1}) and ***b-*** Δf–E dependencies of PEDOT/MnO_2(600) electrode in: ***1***. 1M $LiClO_4$; ***2.*** 1M $NaClO_4$

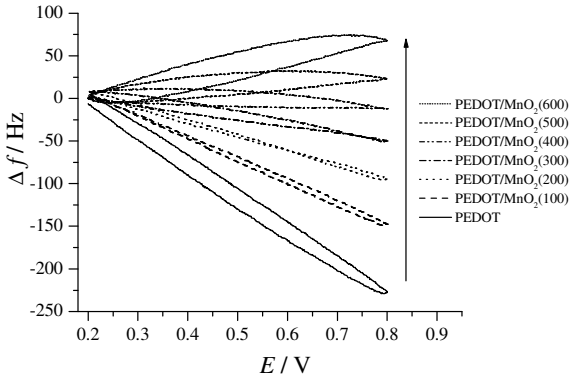

Fig.7 Δ*f*–*E* dependencies for PEDOT and PEDOT/MnO_2 composite films with different times of consecutive MnO_2 deposition. MnO_2 deposition time for each new deposition step was 100s, v = 10 mV s^{-1}